



Pergamon

Acta Materialia 50 (2002) 2945–2954



www.actamat-journals.com

Linear bubble model of abnormal grain growth

W.W. Mullins^a, Jorge Viñals^{b,*}

^a Department of Materials Science and Engineering, Carnegie Mellon University, Pittsburgh, PA 15213-3890, USA

^b Laboratory of Computational Genomics, Donald Danforth Plant Science Center, 975 North Warson Road, St. Louis, MO 63132, USA

Received 30 October 2001; accepted 6 February 2002

Abstract

A linear bubble model of grain growth is introduced to study the conditions under which an isolated grain can grow to a size much larger than the surrounding matrix average (abnormal growth). We first consider the case of bubbles of two different types such that the permeability of links joining unlike bubbles is larger than that of like bubbles (a simple model of grain boundary anisotropy). Stable abnormal growth is found both by mean field analysis and direct numerical solution. We next study the role of grain boundary pinning (e.g., due to impurities or precipitate phases) by introducing a linear bubble model that includes lower and upper thresholds in the driving force for bubble growth. The link permeability is assumed finite for driving forces above the upper threshold, zero below the lower threshold, and hysteretic in between. Abnormal growth is also observed in this case. © 2002 Acta Materialia Inc. Published by Elsevier Science Ltd. All rights reserved.

Keywords: Abnormal grain growth; Grain boundary anisotropy

1. Introduction

We use a linear bubble model of grain growth, originally developed to study self-similar particle coarsening or the development of texture, to investigate possible causes of abnormal grain growth. While the bubble model is a simple idealization of grain growth, it has the advantage that the results obtained are not limited by the mean field approximation inherent to other existing treatments of abnormal growth.

In normal grain growth thermal annealing of a

polycrystalline material results in self-similar coarsening driven by excess free energy reduction. An invariant distribution of scaled grain sizes develops, with an average grain size that grows as a power law of time with a characteristic exponent of 1/2 [1,2,3,4,5]. In abnormal grain growth, on the other hand, a subset of the ensemble of grains grows faster than the surrounding matrix, until the eventual removal of the latter from the distribution. It is a common experimental observation that the distribution of grains that do not exhibit preferential growth stagnates, while the favored subset grows (secondary grain growth). The ensuing particle size distribution function becomes strongly bimodal. When secondary growth completes, the average size of the remaining grains can be much

* Corresponding author.

E-mail address: jvinals@danforthcenter.org (J. Viñals).

larger than that of the initial distribution. An example of a system in which abnormal growth is ubiquitous concerns thin films [6]. Anisotropy of grain boundary properties or elastic strain energies that couple to the orientation of the film grains lead to preferential motion of certain orientations, while constraining others. This dynamical selection of texture leads to a narrow, and often stationary, distribution of grain orientations.

Different mechanisms have been proposed for abnormal grain growth, although the actual physical mechanism responsible for this phenomenon remains largely unknown. Defect induced strains can induce isolated grain growth [7], as well as the same capillary forces responsible for coarsening when anisotropy of grain boundary energies or mobilities exist [8,9]. The conditions for abnormal growth due to variable surface energies or mobilities were recently examined in [10] within a mean field treatment of the matrix grains. For the case of a single grain with boundary properties that differ from those of the surrounding matrix, it was found that a higher boundary mobility generally promotes abnormal growth whereas a higher boundary energy constrains it. The detailed behavior can be quite complex depending on the ranges of the model parameters chosen. It includes abnormal growth only up to a limiting grain size, or lower bounds in the initial size of the grain for abnormal growth to occur.

Abnormal grain growth has also been shown to occur when grain boundaries pin due to, for example, existing precipitate phases or other defects. Simplified models have been proposed that introduce grain boundary drag forces that lead to ultimate pinning (Zener pinning) [11,12], while the role of thermal fluctuations to overcome pinning has been analyzed by Monte Carlo simulation [13].

A number of simplified models of grain growth have been introduced that focus on certain aspects of the problem while simplifying others. Statistical theories have been recently reviewed in [14]. A configuration of the polycrystalline material is described by the (one point) probability distribution of grain sizes and orientations. Phenomenological laws for the average growth velocity of a class of sizes and orientations is introduced to yield a closed set of equations. The topology of the grain

distribution only enters the description in terms of averages, and correlations between neighboring grain sizes and orientations are absent. On the other hand, Monte Carlo simulations based on the Potts model [15,16,17] simplify the grain structure by assigning a single discrete value (“spin”) to the grain orientation, and the grain boundary structure and its energy by introducing a single coupling constant between adjacent spins that represents the (constant) boundary energy. The model, however, incorporates the microstructure topology and correlations between neighboring grains. Computer simulations of normal growth have shown that the distribution of grain sizes becomes asymptotically scale invariant, and that the average grain size grows as a power law of time with an exponent of 1/2 (parabolic kinetics). A third class of models consider idealized boundaries that evolve according to the rule that the local boundary velocity is proportional to its mean curvature [18,19,20,21,22]. For normal growth, parabolic kinetics and scale invariance of the particle radius distribution have also been obtained by direct numerical solution. The case of abnormal growth has been described more recently in [22]. We focus instead on the so-called bubble models. Previous studies of grain growth by using these models include the case of a froth [23], and the linear bubble model of Hunderi, Ryum and Westengen [24]. In this latter case, not only the grains are idealized spherical domains, but also the topology of the microstructure is further simplified into a linear chain of bubbles that exchange mass only among nearest neighbors. Whereas the model is too crude to provide a reliable description of the physical system, its simplicity allows detailed studies of approximations that are often invoked in more realistic treatments (e.g., correlations effects and strict self-similarity versus slow transients and texture development, [25], or dimensionality effects [26]).

Orientation effects and anisotropy in grain boundary energies and mobilities have been introduced into most of the simplified descriptions of grain growth, including statistical theories [14], Potts model simulations [27], moving boundary models [22], and linear bubble models [28,29]. Rollet et al. [27], for example, considered the case

of two distinct orientations by introducing into their Potts model simulation two types of grains and allowing both boundary energy and mobility to depend on whether two adjacent grains are of the same or different type. They used the model to study abnormal grain growth by considering initial conditions for the simulation in which a minority of grains of one type were embedded in a matrix of the other. When boundaries among unequal type grains were assumed to have larger energies or mobilities, abnormal growth was observed, with average radius sizes growing faster than $t^{1/2}$. Orientation effects have been introduced into bubble models of grain growth by Novikov [28], and later by Abbruzzese and Lücke [29] to study the development of texture. Both in Novikov's work and in later work [30,31,25] two types of bubbles A and B were considered to represent the idealized situation of only two different grain orientations. The mobility of unequal A–B boundaries was assumed to be larger than the mobility of either A–A or B–B boundaries. The conditions under which a steady state distribution is reached in this binary case was studied in [25].

We consider in this paper a linear bubble model of grain growth to investigate the conditions that could promote abnormal growth in the model. As is the case with the other simplified models of grain growth, only some generic features of the results are expected to apply to the physical system. In our case, these include the observation that anisotropy in boundary mobility leads to a stable fixed point characterized by a constant ratio between the radius of the abnormal grain to that of the matrix. Our study proves that, within our model, this result is not restricted to the mean field approximation, but that it also holds when correlations between neighboring bubbles are included. We therefore suggest that extending previous mean field treatments of abnormal grain growth to allow for correlations among neighboring grains would not modify this conclusion. We are also able to demonstrate a novel mechanism for abnormal growth in the model. Hysteresis in bubble mobility can lead to abnormal growth, even in the absence of mobility contrast between bubble type. We further show that there is a sharp transition between stagnation and abnormal growth at a criti-

cal value of the lower cut-off for the mobility. We suggest that both features will be present in more realistic models of grain growth. Unfortunately, it is not clear to us at present what is the origin of the hysteresis in mobility, nor how the value of the mobility cut-off can be related to parameters of the physical system.

Section 2 presents a mean field analysis along the lines of the mean field treatment of grain growth by Rollet and Mullins [10]. We consider a linear chain of bubbles of two types to model grain boundary anisotropy and, consistent with their analysis, show that abnormal bubble growth is possible when the permeability of links separating unlike bubbles is larger than that of like bubbles. This mean field analysis is complemented by a direct numerical solution of the model that confirms the mean field predictions regarding abnormal bubble growth: parabolic kinetics for both the abnormal bubbles and the matrix, and a constant value of the ultimate ratio of abnormal to matrix bubble radii.

We then explore in Section 3 a different mechanism that can lead to abnormal growth even for the case of a single bubble type (i.e., in the absence of mobility anisotropy). We model grain boundary pinning by introducing a finite threshold in the driving force for bubble growth. Links between adjacent bubbles are open if the driving force exceeds an upper threshold, and closed if it falls below a lower threshold. In between the two thresholds we assume hysteretic behavior of the link permeability. A numerical solution of the model shows that abnormal growth follows from an initial steady state distribution of bubble sizes depending on the values of the upper and lower thresholds. While the upper threshold largely determines the subset of bubbles that can grow against the matrix, we show that there is a sharp transition in behavior depending on the value of the lower threshold. Abnormal growth is observed below a critical value, with the average radius of the bubbles growing linearly with time. Above this value, the bubble distribution freezes after an initial transient (growth stops).

2. Asymmetric linear bubble model

A linear bubble model of abnormal grain growth is introduced to address the relationship between stable abnormal growth and anisotropic grain boundary mobility. The analysis is motivated by recent research that involved the idealized situation in which a single isolated grain A grows in a matrix of B grains [10]. Under the assumptions that the A – B boundary has a different energy and mobility than B – B boundaries, that the boundary vertices are in equilibrium, and a mean field treatment of the B grain matrix, it was concluded that abnormal grain growth is to be observed when unequal boundaries have higher mobility than equal boundaries, whereas higher surface energy of unequal boundaries relative to equal boundaries constrains it. The linear bubble model described here allows us to extend these results beyond the mean field approximation for the matrix. We find that the conclusion that abnormal growth occurs when unequal boundaries have higher mobility also holds in this case, and that a mean field prediction of the ultimate size ratio is in reasonable agreement with the results of the numerical calculations.

We consider a set of N spherical bubbles of radii R_i , $i=1, \dots, N$, forming a linear chain with periodic boundary conditions. The temporal evolution of the linear bubble model is defined by the following set of equations,

$$\frac{dR_i(t)}{dt} = M_{i\ i+1} \left(\frac{1}{R_{i+1}} - \frac{1}{R_i} \right) + M_{i\ i-1} \left(\frac{1}{R_{i-1}} - \frac{1}{R_i} \right), \quad (1)$$

where M_{ij} is a permeability coefficient between bubbles i and j (the analog of the mobility in the grain boundary case). We first consider in this section the case of two types of grains, A and B , such that $M_{AA}=M_{BB}=1$, and define $\mu=M_{AB}/M_{BB}$. A general property of equation (1) is the existence of a conserved quantity, $\sum_{i=1}^N R_i$, which is independent of time.

Numerical results for the symmetric case $\mu=1$ were given in [25]. For a random initial distribution of bubble radii, the ensemble coarsens

through growth of bubbles larger than a time dependent critical radius, and shrinkage and disappearance otherwise. Following an initial transient, the configuration reaches a stationary self-similar state. In it, consecutive configurations of the coarsening structure are geometrically similar in a statistical sense. As a consequence, any linear scale of the structure (i.e., the average bubble radius) grows as a power law of time

$$\langle R(t) \rangle^2 - \langle R(t_0) \rangle^2 = C(t-t_0),$$

where $\langle \rangle$ denotes the configuration average, and t_0 is some time in the self-similar regime.

We now turn to the asymmetric case of $\mu>1$ in the limit of a small fraction of A bubbles. Before presenting the results of our numerical calculations for $\mu>1$, we discuss a mean field treatment of the linear bubble model (equation (1)) along the same lines of [10], and show that similar conclusions follow. We then obtain a numerical solution of equation (1), and demonstrate that, in agreement with the mean field results, the linear bubble model does lead to abnormal grain growth when $\mu>1$. We also show that the ultimate size ratio between the abnormal grains and the matrix is quite close to that predicted by the mean field analysis.

Consider a single bubble of type A in a long chain of B bubbles, and that the AB links have a mobility $M_{AB} \neq M_{BB}$, with the mobility ratio $\mu=M_{AB}/M_{BB}$. Since the number of B bubbles is large, the evolution of the matrix will not be appreciably affected by the presence of the abnormal A bubble. Furthermore, since $R_A \gg \langle R_B \rangle$, matrix bubbles adjacent to A will quickly shrink to zero in the characteristic time scale for growth of matrix bubbles. Hence we expect that the radius distribution of B bubbles that become neighbors of the growing A bubble will be well approximated by that which corresponds to normal growth of matrix bubbles. We therefore approximate the time dependence of $\omega = R_A/\langle R_B \rangle$ by using a mean field approximation to the evolution of the B bubbles. We start from,

$$\langle \dot{\omega} | \omega \rangle = \frac{d}{dt} \left(\frac{R_A}{\langle R_B \rangle} \right) = \frac{1}{\langle R_B \rangle^2} \left[\langle R_B \rangle \langle \dot{R}_A | R_A \rangle - R_A \frac{d\langle R_B \rangle}{dt} \right]. \quad (2)$$

Since the A bubble has two B bubbles as neighbors, one has,

$$\langle \dot{R}_A | R_A \rangle = 2M_{AB} \left[\left\langle \frac{1}{R_B} \right\rangle - \frac{1}{R_A} \right] = 2M_{AB} \left[\frac{\alpha}{\langle R_B \rangle} - \frac{1}{R_A} \right], \quad (3)$$

where the second equality follows from assuming self-similarity of the matrix bubbles and $\alpha = \langle R_B \rangle \langle 1/R_B \rangle = \langle R_B \rangle / R_c \approx 1.1927$ (cf. Appendix A). Only weak deviations from self-similarity are expected for the matrix distribution under the conditions of our study. We do not address, however, the consequences of a finite number fraction of abnormal grains, nor its effect on the growth of the ensemble.

The mean field treatment of the B bubbles outlined in Appendix A gives for the critical radius $R_c = M_{BB}/2R_c$, and hence from the definition of α we find,

$$\frac{d\langle R_B \rangle}{dt} = \frac{M_{BB}\alpha^2}{2\langle R_B \rangle}. \quad (4)$$

Substituting equations (3) and (4) into equation (2) gives,

$$\langle \dot{\omega} | \omega \rangle = \frac{M_{BB}}{\langle R_B \rangle^2} G(\mu, \omega), \quad (5)$$

where,

$$G(\mu, \omega) = 2\mu \left(\alpha - \frac{1}{\omega} \right) - \frac{\alpha^2 \omega}{2}. \quad (6)$$

This latter function determines the sign of $\langle \dot{\omega} | \omega \rangle$, and therefore whether the A bubble grows or shrinks relative to the coarsening B matrix.

For $\mu=1$ the function G is everywhere non-positive. For $\mu>1$ there is a range of values of ω for which G is positive, and in particular a stable fixed point at some $\omega=\omega_+$ that corresponds to steady abnormal growth. Figure 1 shows the phase space plot of $\dot{\omega}$ for $\alpha = 1$ and $\mu = 1.5$. For values of ω from roughly 1 to 4, $\dot{\omega} > 0$ so that a bubble of type A in this range would grow relative to the matrix of B bubbles. However, if the ratio ω exceeds 4, the larger bubble would shrink back to the fixed point. This root of G is a stable fixed

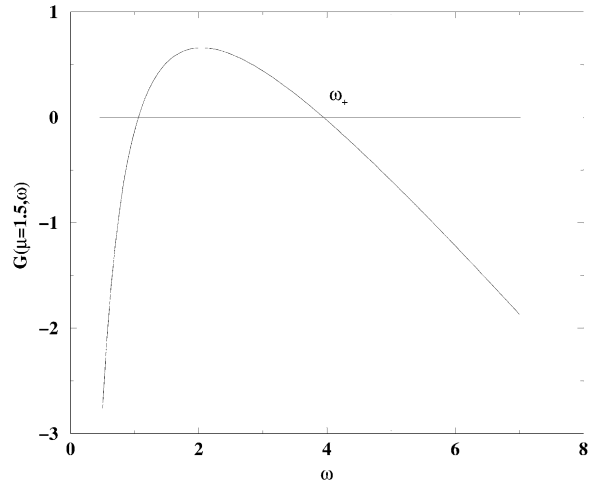


Fig. 1. Phase plot $\dot{\omega}$ versus ω where $\omega = R_A/\langle R_B \rangle$ is the ratio between the radius of the A and matrix bubbles. $G>0$ corresponds to ratio growth, and $G<0$ otherwise. The plot shows two fixed points ($G=0$) at two different values of ω . The smallest of the two is unstable, and the largest, denoted by ω_+ is stable. This is the expected operating point of the model and corresponds to a fixed size ratio between R_A and $\langle R_B \rangle$.

point. The other root $\omega \approx 1$ is not stable. The upper root of $G(\mu, \omega)$ is given by,

$$\omega_+ = \frac{2}{\alpha} (\mu + \sqrt{\mu^2 - \mu}). \quad (7)$$

The range of relative growth is given by the difference between the upper and lower roots of equation (6),

$$\Delta\omega = \frac{4}{\alpha} \sqrt{\mu^2 - \mu}. \quad (8)$$

We next compare the results of the mean field calculation to a direct numerical solution of the set of equation (1). We only describe the algorithm briefly, further details can be found in [25]. We consider a large number of bubbles $N=2 \times 10^6$, and impose periodic boundary conditions such that $R_{N+1}(t)=R_1(t)$. We initially place 20 equally spaced bubbles of type A in a matrix of $N-20$ bubbles of type B. The initial sizes of B bubbles are distributed according to the mean field distribution (equation (A9) with $\langle R_B \rangle(t=0) = 5$). The initial radius of the A bubbles is fixed at $R_A(t=0) = 3\langle R_B \rangle(t=0)$ for the results presented in this section. A wide range of initial ratios has been investi-

gated with identical results. We also set $M_{BB}=1$. A lower size cut-off R_{\min} is introduced for numerical reasons so that any bubble for which $R_i(t) \leq R_{\min}$ during the course of the calculation is removed, and the two adjacent bubbles redefined as neighbors. The value of $R_{\min}=0.28$ is chosen so that no bubble can shrink to zero in $\Delta t=0.02$, the time discretization used to integrate the system of equations (1). The averages shown refer only to averages over the configuration. We have not performed additional averages over independent initial conditions as the large number of bubbles considered appears to be sufficient for the required statistical accuracy.

Figure 2 shows our results for $\langle R_B(t) \rangle$ as well as $\langle R_A \rangle$, where the latter is an average over the 20 bubbles of type A. The average radius of the matrix bubbles $\langle R_B(t) \rangle$ exhibits power law growth with an exponent of 1/2, in agreement with the mean field prediction of Appendix A. The figure also shows two least square fits to obtain the corresponding amplitudes of the power laws which are used to calculate the ratio $\langle R_A \rangle / \langle R_B \rangle$ at long times. Figure 3 shows our numerical results for the ratio of amplitudes for a range of mobility ratios μ , and compares them with the mean field prediction given by equation (7).

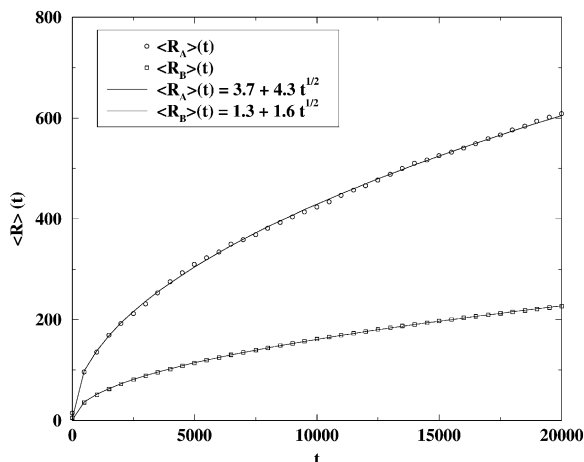


Fig. 2. Average radius of large bubbles $\langle R_A \rangle$, and average radius of the matrix $\langle R_B \rangle$ as a function of time for a mobility ratio $\mu=1.5$. Both A and B bubbles exhibit average parabolic growth to a very good approximation as shown by the fits (solid lines). The amplitudes of the term $t^{1/2}$ are used to estimate the quantity ω_+ shown in Fig. 3 for each value of μ .

In summary, a mean field treatment of the linear bubble model with unequal boundary mobilities predicts that abnormal bubble growth will occur for $\mu > 1$ with an ultimate size ratio of ω_+ . The numerical results confirm power law growth in time of both A and B average radii, with an exponent of 1/2. The numerical results for the ultimate size ratio ω_+ are also in excellent agreement with the mean field prediction. Clearly, bubble size correlations that are not taken into account in the mean field treatment must only introduce small corrections.

3. Symmetric case with a mobility threshold

We investigate in this section a different mechanism leading to abnormal grain growth even in the absence of any mobility anisotropy. We hypothesize that if a finite threshold to grain boundary motion exists, then it is possible that a large fraction of the matrix grains would remain immobile, except for those that were sufficiently larger than their neighbors so that the local driving force for growth exceeds the given threshold. The excess energy that is contained in the initial particle distribution would then be relieved mostly

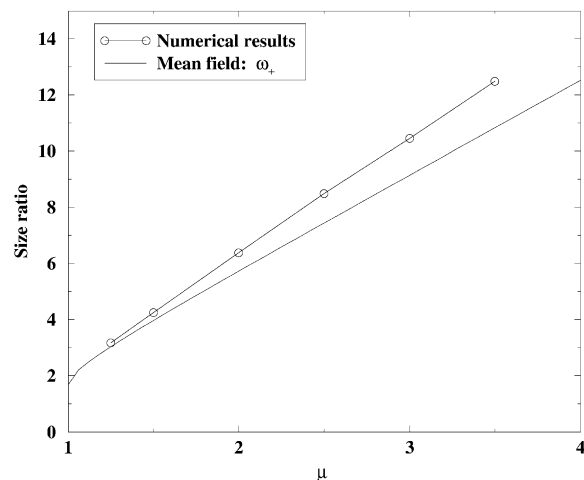


Fig. 3. (○), values of ω_+ obtained by numerical integration. For each value of the mobility ratio μ the model equations are integrated in time, and the value of ω_+ estimated by fitting parabolas to the average radii as shown in Fig. 2. The solid line is the mean field prediction, equation (7).

through size increases of the larger grains at the expense of a largely immobile, high energy, matrix distribution.

In order to investigate this possibility within the linear bubble model introduced in Section 2, we consider an ensemble of like bubbles and introduce two threshold values for the mobility M in equation (1). Let $\Delta p = 1/R_i - 1/R_{i+1}$ be the local driving force associated with the i th link, and $\Delta p_l < \Delta p_u$ the low and high driving force thresholds, respectively. We define $M = 1$ if $|\Delta p| > \Delta p_u$, and $M = 0$ if $|\Delta p| < \Delta p_l$. We also assume a hysteresis loop in $\Delta p_l < |\Delta p| < \Delta p_u$ with $M = 0$ in the lower branch and $M = 1$ in the upper branch. Therefore a link remains closed ($M = 0$) until $|\Delta p|$ across the link exceeds Δp_u . Once the link is open ($M = 1$) it remains open until $|\Delta p|$ falls below Δp_l . Finally, when a bubble radius falls below R_{\min} , so that the bubble is removed from the distribution, a new link between the new neighboring bubbles is made, and its mobility is assigned to be 1 unless $|\Delta p| < \Delta p_l$.

We have used the same numerical algorithm described in Section 2 to integrate the system of equation (1) with the mobility thresholds just introduced. In this Section we consider an ensemble of $N = 10^6$ identical bubbles, initially distributed according to the mean field result, equation (A9), with $\langle R(t = 0) \rangle = 5$. Although all bubbles are identical in the present case, it is convenient for the sake of the discussion to refer to those that grow relative to the average as A bubbles, and as B or matrix bubbles to the rest.

Figure 4 shows our results for the bubble radius distribution function for a representative set of parameters $\Delta p_l = 0.05$ and $\Delta p_u = 3.0$. Even though all bubbles are identical and follow the mean field distribution at $t = 0$, the largest bubbles in the initial ensemble grow while most of the rest remain stagnant. This figure shows the radius distribution $p(R)$ (with the main peak near $R = \langle R \rangle$ suppressed for clarity) starting at $t = 1000$ all the way up to $t = 25000$ in increments of 2000 time units. It is clear from the figure that a small subset of the initial distribution grows as indicated by the successive peaks of $p(R)$ at large R .

Not all possible combinations of Δp_l and Δp_u result in abnormal growth however. First, there is

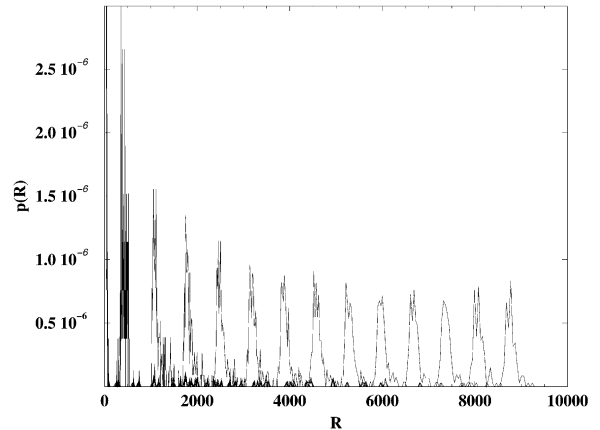


Fig. 4. Probability distribution function of particle radius as a function of R for several times ranging from $t = 1000$ to $t = 25000$ in increments of 2000 time units. The main peak of the distribution has been removed for clarity. Each of the peaks shown at large R corresponds to a specific time, and they are ordered from left to right according to increasing times. The distributions show the existence of a small set of large bubbles that grow to a size much larger than the matrix average.

an obvious upper bound for Δp_u given the initial radius distribution, and it corresponds to the driving force Δp between the largest possible bubble $R_{\max} \approx 8.4$ for our initial distribution, and $R_{\min} \approx 0.28$. We find $\Delta p_{\max} = 1/R_{\min} - 1/R_{\max} \approx 3.42$. If $\Delta p_u > \Delta p_{\max}$ no bubble will grow.

For fixed $\Delta p_u < \Delta p_{\max}$, a bubble will grow (call it A) at the expense of a B neighbor when $R_A > (1/R_B - \Delta p_u)^{-1}$. Therefore for a given initial distribution the value of Δp_u determines the range of radii of bubbles expected to grow. Once a given A bubble starts growing, it will only stop if it encounters a bubble B such that $1/R_B - 1/R_A < \Delta p_l$. Equivalently, whenever an A bubble encounters a bubble of radius $R_B = (1/R_A + \Delta p_l)^{-1}$ or larger, growth will stop. If one further assumes that growth of A has already occurred for some time so that R_A is sufficiently large, then this condition is approximately $R_B \approx 1/\Delta p_l$ independent of R_A , a relation that can be used to define a critical value for growth Δp_l^c . If $\Delta p_l \geq \Delta p_l^c$ there is a nonzero probability that a large and growing A bubble will become the neighbor of a B bubble that is sufficiently large to stop growth of the A bubble. If the matrix has remained approximately stagnant, this critical value can be obtained from $R_{\max} \approx 8.4$ as $\Delta p_l^c =$

$1/R_{\max} \approx 0.12$ (in practice, the numerically sampled initial condition typically has $R_{\max} \approx 7.9$ or $\Delta p_1^c \approx 0.127$). This behavior is observed numerically and is illustrated in Fig. 5. The figure shows the radius of the largest bubble in the ensemble as a function of time. The upper cut-off in all the cases shown is fixed $\Delta p_u = 2.0$, and the figure shows the results for a range of values of Δp_1 . The value $\Delta p_1 \approx 0.130$ marks the transition between abnormal growth and an ultimately frozen configuration. Note that the transition is quite sharp as a function of Δp_1 . Identical numerical results concerning this transition as well as the same critical value Δp_1^c have been obtained for $\Delta p_u = 2.5$ and $\Delta p_u = 3.0$.

In summary, the upper cut-off Δp_u determines the fraction of the ensemble that can grow, and therefore the degree of stagnation of the matrix. Once abnormal grain growth has started, the value of the lower cut-off Δp_1 (and the amount of growth in the matrix, if any) determines whether abnormal growth continues or rather the system reaches a frozen configuration.

We finally mention that while abnormal growth occurs, the typical radius R_A of the large particles is expected to grow linearly with time. In mean

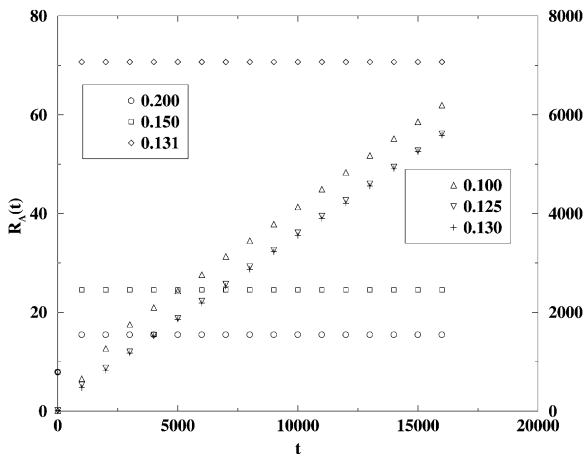


Fig. 5. Largest bubble radius in the distribution as a function of time. The upper threshold $\Delta p_u = 2.0$ in all the cases shown, and the values of the lower thresholds are indicated in the figure. The three largest values of $\Delta p_1 = 0.131, 0.150$ and 0.200 lead to an asymptotically stagnant configuration (left axis), whereas the values $\Delta p_1 = 0.100, 0.125$ and 0.130 lead to abnormal growth (right axis).

field, a given A bubble will have two B bubbles as nearest neighbors and therefore

$$\frac{dR_A}{dt} = 2M_{AB} \left(\frac{1}{R_B} - \frac{1}{R_A} \right). \tag{9}$$

While bubble A grows successive B neighbors will shrink to zero and be eliminated from the ensemble. Therefore the growth of A can be estimated by averaging equation (9) over the distribution of B, and when the matrix is almost stagnant, over the initial distribution of bubble radii. In either case, $\langle 1/R_B \rangle$, where $\langle \rangle$ denotes average over the configuration, will be constant (or changing very slowly compared with the rate of growth of the A bubble), so that for sufficiently long times ($1/R_A \ll \langle 1/R_B \rangle$) $dR_A(t)/dt$ is approximately constant. This is the dependence shown in Fig. 5 in the cases in which abnormal grain growth is observed. The value of the slope of the line $R_A(t)$ versus t can be straightforwardly obtained by computing the average $\langle M_{AB}/R_B \rangle \langle M_{AB}/R_B \rangle$ over the initial distribution of matrix grains.

Acknowledgements

This research has been supported by the US Department of Energy, contract No. DE-FG05-95ER14566.

Appendix A. A Mean field calculation for a linear bubble model undergoing normal growth

Consider a set of identical spherical bubbles arranged along a line that model a set of neighboring (identical) grain boundaries. The equation of motion for their radii is,

$$\frac{dR_i}{dt} = M \left(\frac{1}{R_{i+1}} + \frac{1}{R_{i-1}} - \frac{2}{R_i} \right). \tag{A1}$$

Average equation (A1) over the ensemble of bubbles. The left hand side will be simply denoted by $\langle \dot{R}_i | R_i \rangle$, the average growth rate of a particle of radius R_i . The right hand side is treated at the mean field level (i.e., neglecting correlations) so that

$\langle 1/R_{i+1} \rangle = \langle 1/R_{i-1} \rangle = \langle 1/R \rangle$, the average of $1/R$ over the set. We now use this latter quantity to define a time dependent critical radius $1/R_c = \langle 1/R \rangle$ so that bubbles of radius large than R_c will grow, and shrink otherwise. The mean field approximation to equation (A1) is,

$$\langle \dot{R}_i | R_i \rangle = 2M \left(\frac{1}{R_c} - \frac{1}{R_i} \right). \tag{A2}$$

Define now a reduced radius $r=R/R_c$. Equation (A2) can also be written as,

$$R_c \langle \dot{R}_i | R_i \rangle = 2M \left(1 - \frac{1}{r} \right). \tag{A3}$$

As is standard in the analysis of steady state solutions for the averages [32], one first defines the quantity,

$$y = \dot{R}_c R_c = \frac{1}{2} \frac{dR_c^2}{dt},$$

so that equation (A1) can be written as,

$$R_c^2 \langle \dot{r} | r \rangle = f(r) - ry, \tag{A4}$$

where we have defined $f(r)=2M(1-1/r)$. This equation is a particular case of equation (7) in [32]. The nodal curve defined by $\langle \dot{r} | r \rangle = 0$ is thus given in our case by,

$$y = 2M \left(\frac{1}{r} - \frac{1}{r^2} \right). \tag{A5}$$

According to the classical mean field treatment of Lifshitz and Slyozov [33], there exists a stable operating point of the reduced particle size distribution determined by equation (A1) that corresponds to the maximum of the nodal curve $y=y_m$, so that the distribution of reduced radii r extends from $r=0$ to a sharp cutoff $r=r_m$. For our particular form of the nodal curve, equation (A5), we have $r_m=2$, and $y_m=M/2$. A statistical self-similar distribution is reached with this value of y , and from its definition, we have,

$$\frac{dR_c}{dt} = \frac{M}{2R_c},$$

that after integration leads to the asymptotic parabolic growth law,

$$R_c^2(t) - R_c^2(t_0) = \frac{M}{2}(t - t_0),$$

where t_0 is some time within the self-similar regime.

The distribution of reduced particle sizes can also be computed by using our result for $f(r)$, and equation (14) in [32]. Define the function $F(r) = t \langle \dot{r} | r \rangle$, which satisfies in the steady state,

$$F(r) = \frac{f(r) - ry_m}{2y_m} = -\frac{(2-r)^2}{2r}. \tag{A6}$$

The general solution of the continuity equation for $n(r,t)$, the number particle density, is given by [32],

$$n(r,t) = \frac{1}{F(r)} \Psi[t - \Theta(r)],$$

where Ψ is an arbitrary function and where,

$$\Theta(r) = \int_0^r \frac{dr'}{F(r')}. \tag{A7}$$

Substitution of equation (A6) into equation (A7) yields,

$$\Theta(r)/2 = -\ln(2-r) - \frac{2}{2-r} + \ln 2 + 1. \tag{A8}$$

With this result, the normalized probability distribution function $P(r) = n(r,t) / \int n(r,t) dr$ is time independent and given by (equation (20) in [32]),

$$P(r) = \frac{2e}{(2-r)^3} e^{-2/(2-r)}, \quad 0 \leq r \leq r_m \tag{A9}$$

We note that the upper cut-off is $r_m=2$, that the maximum of $P(r)$ occurs at $r = \sqrt{2}$, and that the average reduced radius is given by $\langle r \rangle = \langle R \rangle / R_c \approx 1.1927$.

References

- [1] Burke J. Trans metall Soc AIME 1949;180:73.
- [2] Smith C. In: Metals interfaces. Cleveland, OH: American Society for Metals; 1952. p. 6-5.
- [3] Burke J, Turnbull D. Prog Metal Phys 1952;3:220.

- [4] Mullins W. *J Appl Phys* 1956;27:900.
- [5] Mullins W. *Acta mater* 1998;46:6219.
- [6] Thompson C. *Interface Sci* 1998;6:85.
- [7] Rollett A, Srolovitz D, Anderson M, Doherty R. *Acta metall* 1992;40:3475.
- [8] Rollett A, Srolovitz D, Anderson M. *Acta metall* 1989;37:1227.
- [9] Grest G, Anderson M, Srolovitz D, Rollett A. *Scripta metall* 1990;24:661.
- [10] Rollett A, Mullins W. *Scripta materialia* 1997;36:975.
- [11] Hillert M. *Acta metall* 1965;13:227.
- [12] Anderson I, Gront O, Ryum N. *Acta metall mater* 1995;43:2689.
- [13] Messina R, Soucail M, Kubin L. *Met Sci Eng A—Struct* 2001;308:258.
- [14] Lucke K, Brandt R, Abbruzzese G. *Interface sci* 1998;6:67.
- [15] Srolovitz D, Grest G, Anderson M. *Acta met* 1985;33:2233.
- [16] Vinals J, Gunton J. *Phys Rev B* 1986;33:7795.
- [17] Anderson GGMP, Srolovitz D. *Phil Mag B* 1988;59:293.
- [18] Ceppi E, Nasello O. *Scripta metall* 1984;18:1221.
- [19] Fradkov V, Shvindlerman L, Udler D. *Scripta metall* 1985;19:1285.
- [20] Frost H, Thompson C, Howe C, Wang J. *Scripta metall* 1988;22:65.
- [21] Beenakker C. *Phys Rev A* 1987;37:1697.
- [22] Novikov V. *Interface Sci* 1998;6:77.
- [23] Wejchert J, Wearie D, Kermode J. *Phil mag B* 1986;53:15.
- [24] Hunderi O, Ryum N, Westengen H. *Acta metall* 1978;27:161.
- [25] Mullins W, Vinals J. *Acta metall mater* 1993;41:1359.
- [26] Vinals J, Mullins W. *J Appl Phys* 1998;83:621.
- [27] Rollet A, Srolovitz D, Anderson M. *Acta metall* 1989;37:1227.
- [28] Novikov V. *Acta metall* 1979;27:1461.
- [29] Abbruzzese G, Lucke K. *Acta metall* 1986;34:905.
- [30] Eichelkraut H, Abbruzzese G, Lucke K. *Acta metall* 1988;36:55.
- [31] Abbruzzese G, Lucke K, Eichelkraut H. *Trans ISIJ* 1988;28:818.
- [32] Mullins W. *Acta metall* 1991;39:2081.
- [33] Lifshitz I, Slyozov V. *J Phys Chem Solids* 1961;19:35.